# Self Assembly of Coiled-Coil Peptide−Porphyrin Complexes

Bashkim Kokona, Andrew M. Kim, R. Claire Roden, Joshua P. Daniels, Brian J. Pepe-Mooney, Brian C. Kovaric, Julio C. de Paula,[§] Karl A. Johnson, and Robert Fairman*

*Department of Biology, Haverford College, 370 Lancaster Avenue, Haverford, Pennsylvania 19041*

*Received January 14, 2009; Revised Manuscript Received March 13, 2009*

We are interested in the controlled assembly of photoelectronic materials using peptides as scaffolds and porphyrins as the conducting material. We describe the integration of a peptide-based polymer strategy with the ability of designed basic peptides to bind anionic porphyrins in order to create regulated photoelectronically active biomaterials. We have described our peptide system in earlier work, which demonstrates the ability of a peptide to form filamentous materials made up of self-assembling coiled-coil structures. We have modified this peptide system to include lysine residues appropriately positioned to specifically bind *meso*-tetrakis(4-sulfonatophenyl)porphine ($TPPS_4$), a porphyrin that contains four negatively charged sulfonate groups at neutral pH. We measure the binding of $TPPS_4$ to our peptide using UV−visible and fluorescence spectroscopies to follow the porphyrin signature. We determine the concomitant acquisition of helical secondary structure in the peptide upon $TPPS_4$ binding using circular dichroism spectropolarimetry. This binding fosters polymerization of the peptide, as shown by absorbance extinction effects in the peptide CD spectra. The morphologies of the peptide/porphyrin complexes, as imaged by atomic force microscopy, are consistent with the coiled-coil polymers that we had characterized earlier, except that the heights are slightly higher, consistent with porphyrin binding. Evidence for exciton coupling in the copolymers is shown by red-shifting in the UV−visible data, however, the coupling is weak based on a lack of fluorescence quenching in fluorescence experiments.

## Introduction

Protein self-assembly has been recognized as a powerful paradigm for the creation of biomaterials that can be engineered with atomic precision and can be regulated by environmental conditions. The focus here is on imparting photoelectronic activity onto peptide-based structural scaffolds. The use of porphyrins and hemes as photoelectronic modules has been extensively studied and several reviews have been published describing these efforts.[1−3] The electronic properties of porphyrins have also been studied bound to other biomacromolecules, such as DNA,[4,5] carbohydrates,[6] and lipids,[7−9] with an eye to developing biomaterials with photoelectronic properties. The advantage in using protein-based scaffolds is the ability to regulate assembly and disassembly of biomaterials by using the diverse functionality afforded by both natural and unnatural amino acids.

Protein design efforts have focused largely on taking advantage of side-chain functional groups to coordinate the metal ions bound to various porphyrin structures;[2] we instead take advantage of noncovalent binding between porphyrin pendant groups and amino acid functional groups as this would allow greater flexibility to use different metalated porphyrins without compromising design strategies. We have focused on studies involving peptide interactions with *meso*-tetrakis(4-sulfonatophenyl)porphine ($TPPS_4$) by taking advantage of electrostatic interactions with the sulfonate groups.[10] Charged interactions have been demonstrated between $TPPS_4$ and peptides or proteins containing basic amino acids in aqueous solution. These include studies of general binding to proteins such as tubulin,[11] lysozyme,[12] serum albumin,[12,13] and α-lactoglobulin.[13]

It is well-known that $TPPS_4$ itself can aggregate at low pH (pH < 2.0), forming either J aggregates or, at higher porphyrin concentration, H aggregates. The structural difference in these aggregates derives from different stacking geometries between porphyrin pairs, in which the J aggregates are thought to form an array of slipped face-to-face stacking interactions.[14] Imaging studies of J aggregates reveal that these linear arrays appear as nanorods in the micrometer scale range;[15−18] little is known about large scale structural properties of H aggregates. These structures have been well characterized by spectroscopic methods. Monomeric $TPPS_4$ has a Soret absorption band at 413 nm at neutral pH. This band is red-shifted to 434 nm in its diacid form at low pH. J aggregates are characterized by a spectroscopic signature containing a strongly red-shifted Soret band at 490 nm (J-band) and a second band at 706 nm ($Q_x$-band).[19,20] H aggregates, in contrast, are characterized instead by a blue-shifted Soret band.[21]

Thus, most of the work involving protein/$TPPS_4$ interactions has been done under these low pH conditions where the porphyrins can self-assemble.[12,13] The focus in the work at low pH has been on how protein binding might regulate the J-aggregate assembly and modulate the relevant electronic transitions. However, at such low pH, many peptides and proteins are susceptible to unfolding, thus, interactions at neutral pH are more appropriate for biomaterials design to maintain the integrity of protein structure.[11,13] Several papers have described charged peptide−porphyrin interactions[22−26] (including $TPPS_4$);[27] these papers explored the ability to couple protein folding and self-assembly with porphyrin interaction. We became interested in such coupling of protein folding upon porphyrin interaction as a mechanism to create biomaterials whose self-assembly is driven, at least in part, by protein structural transitions.[10,28] We have demonstrated that $TPPS_4$ can bind noncovalently to a peptide through interactions between the porphyrin sulfonate groups and appropriately spaced lysine

* To whom correspondence should be addressed. Tel.: (610) 896-4205. Fax: (610) 896-4963. E-mail: rfairman@haverford.edu.

[§] Current Address: Department of Chemistry, Lewis and Clark College, 0615 SW Palatine Hill Rd., Portland, OR 97219.

10.1021/bm9000553 CCC: $40.75 
Published on Web 04/17/2009

**Table 1.** Peptide Sequences[a]

| | *abcdefg abcdefg* | *abcdefg abcdefg* |
|---|---|---|
| CpA | Ac-CKQLEDK IEELLSK AA | CKQLEDK IEELLSK-$CONH_2$ |
| CpA-I | Ac-**I**KQLEDK **I**EELLSK AA | **I**KQLEDK **I**EELLSK-$CONH_2$ |
| Cp3K-N | Ac-IQQL**K**NQ I**K**QLL**K**Q | -$CONH_2$ |
| Cp3K | Ac-IQQL**K**NQ I**K**QLL**K**Q AA | IQQLQNQ IQQLLQQ-$CONH_2$ |

[a] Heptad positions denoted with the letters *a*−*g*.

residues in the peptide.[10] The peptide, Cp3K−N (see sequence in Table 1), contains three lysine residues that are spaced *i*,*i* + 4 with respect to one another. This spacing would juxtapose the lysines to interact with three sulfonate groups upon acquisition of a helical structure (Figure 1). Circular dichroism, UV−visible spectroscopy, and analytical ultracentrifugation experiments from this earlier work demonstrated that the peptide/porphyrin interaction was specific and thus presented an attractive model for precise engineering of photoelectronically active biomaterials.[10]

Toward the goal of developing peptide scaffolds for photoelectronic functionalization, we created a coiled-coil based polymerization strategy that could be combined simply with a porphyrin-binding module as described above and as illustrated in Figure 1.[1,29] Coiled coils are protein structural motifs that take advantage of amphipathic α-helices to drive precise helix-pairing interactions. Most natural and designed coiled coils are hydrophobic along one continuous face of the helix, resulting in well-defined assemblies. However, we modified a sequence that normally creates an amphipathic helix to favor offset helix pairing interactions.[29] This was done by inserting two alanines between two 14-residue amphipathic sequences, placing out of phase the hydrophobic residues in the second half of the sequence by 210° with respect to the first half. Thus, helix pairing would necessitate a staggered structure that could polymerize to form filaments and fibrils in the $10^{-9}-10^{-6}$ meter range. In the past several years, such redesign strategies using coiled coils to form nanoscale biomaterials have been realized and attempts to build functionality and larger-scale structural features are well underway.[1,30−32]

We then re-engineered the polymerizing peptide (CpA) described in our earlier work[29] to incorporate the lysines at the same relative positions as that described for Cp3K-N.[10] This new peptide, which we call Cp3K (Table 1), thus contains elements of CpA and Cp3K-N with some additional modifications; a model of the presumed interaction of Cp3K with $TPPS_4$ is shown in Figure 1. In unpublished work, we found that replacing the cysteines in CpA with isoleucines (CpA-I; Table 1) enhances the hydrophobic interactions between helices and fosters self-assembly at lower peptide and salt concentrations. In addition, the lysines at all other positions and all of the glutamates in our original design were replaced with glutamines to avoid unwanted electrostatic interactions. The work described here shows our efforts to characterize the photoelectronic and structural properties of Cp3K/$TPPS_4$ self-assembled biomaterials.

## Experimental Section

**Molecular Modeling.** The starting molecular model for the coiled-coil polymer was taken from our published model for the 30-residue CpA peptide.[29] The model for the Cp3K-N interaction with $TPPS_4$[10] was then overlaid onto the CpA polymer model in the following way (see Table 1 for the peptide sequences). Using InsightII 2000 (Biosym Technologies, San Diego), the backbone atoms from the central 10 amino acid residues in the Cp3K-N peptide (docked with $TPPS_4$) were superimposed onto the equivalent set of atoms within the first two heptads of CpA. This allowed the $TPPS_4$ to be properly oriented relative to the polymerizing module of CpA. The original Cp3K-N structure was then deleted, leaving only the $TPPS_4$ porphyrin docked onto the CpA sequence. The appropriate residues in CpA were then mutated to lysine residues and these side chains were then manually adjusted to be consistent with their conformations in the original Cp3K-N/$TPPS_4$ model. This exercise was repeated two more times to give a three-module repeating structure as shown in Figure 1.

**Peptide Synthesis and Purification.** The synthesis of Cp3K was carried out on an Applied Biosystems (Foster City, CA) 433A peptide synthesizer using standard FMOC chemistry and using PAL resin (Advanced ChemTech, Louisville, KY), providing an amide at the carboxy-terminus. The peptides were acetylated at the amino terminus prior to TFA cleavage. Peptides were purified using RP-HPLC with a mobile phase of water and acetonitrile and 0.1% TFA on a Varian ProStar (Varian, Inc., Palo Alto, CA) system equipped with a Varian Dynamax semipreparative C18 column. Peptide was collected and lyophilized for long-term storage. The peptide identity was confirmed using MALDI-TOF mass spectrometry, yielding a molecular mass of 3611.8 Da (theoretical MW = 3612.2 Da).

**Solution Preparation.** Lyophilized peptide was dissolved in Milli-Q-filtered water to make stock solutions and used within a few weeks to avoid problems with unwanted aggregation. Peptide stock solution concentrations (1−2 mM) were determined by using a modified ninhydrin procedure from Rosen.[33] Porphyrin stock solutions (<1 mM) were prepared by dissolving $TPPS_4$ (Frontier Scientific Inc.) in 6 mM NaOH and measuring the concentration of this solution using $\varepsilon_{414} = 5.33 \times 10^5\ M^{-1}\ cm^{-1}$.[19]

**Circular Dichroism Spectropolarimetry.** CD data were collected on an Aviv Associates (Lakewood, NJ) model 202-01 CD spectropolarimeter. Wavelength scans were performed at 25 °C in the range of 198−250 nm for the peptide bands and 350−550 nm for the porphyrin bands using a wavelength step size of 1.0 nm. Data points represent 3 s of averaging time. All samples were measured in 10 mM Tris-HCl, pH 7.8, unless stated otherwise.

**UV−Visible Spectroscopy.** UV−visible data were collected using a 1 mm cuvette on a Lambda 25 UV/vis spectrophotometer (Perkin-Elmer Instruments, Waltham, MA). Wavelength scans from 350 to 800 nm were performed at room temperature, using a wavelength step size of 1.0 nm. Samples were prepared in 10 mM Tris-HCl, pH 7.8.

**Fluorescence Spectroscopy.** Fluorescence spectroscopy was performed using a 1 cm cuvette on a Fluorolog-2 spectrofluorometer (Spex Industries, Inc., Edison, NJ) under the control of the dedicated SPEX DM3000F software. Fluorescence scans were performed at room temperature in the range of 500 to 800 nm using increments of 1.0 nm, an integration time of 1 s, and an excitation wavelength of 413 nm, which is at the absorption peak maximum for free porphyrin. Samples were prepared in 10 mM Tris-HCl, pH 7.6.

**Fluorescence Microscopy.** Fluorescence microscopy was performed on an Axiophot microscope (Carl Zeiss Inc., Thornwood NY) equipped with a 100 W mercury excitation source and using a D436/20 excitation filter, a D455DCLP dichroic (Chroma Technology, Rockingham, VT), and a 590LP emission filter (XF3016, Omega Optical, Brattleboro VT). Digital images were captured using an Orca ER cooled CCD camera (Hamamatsu Photonics, Bridgewater, NJ) and a Dell computer (Dell Inc., Round Rock, TX) running Windows XP (Microsoft Corp., Seattle, WA) and Metamorph (Molecular Devices, Downingtown, PA) software. Images were converted from 12-bit files into an 8-bit RGB format and cropped and composited using Photoshop (Adobe Systems Inc., San Jose, CA).

**Analytical Ultracentrifugation.** Ultracentrifugation experiments were performed using a Beckman model ProteomeLab XL-A analytical ultracentrifuge (Palo Alto, CA) equipped with an An-60 Ti rotor. Velocity experiments used two-channel Epon charcoal-filled centerpieces with 12 mm path length containing 435 μL of sample and 450 μL of buffer reference. Samples were prepared in 10 mM Tris-HCl, pH 7.8 and 0.1 M NaCl. Sedimentation velocities of peptide boundaries

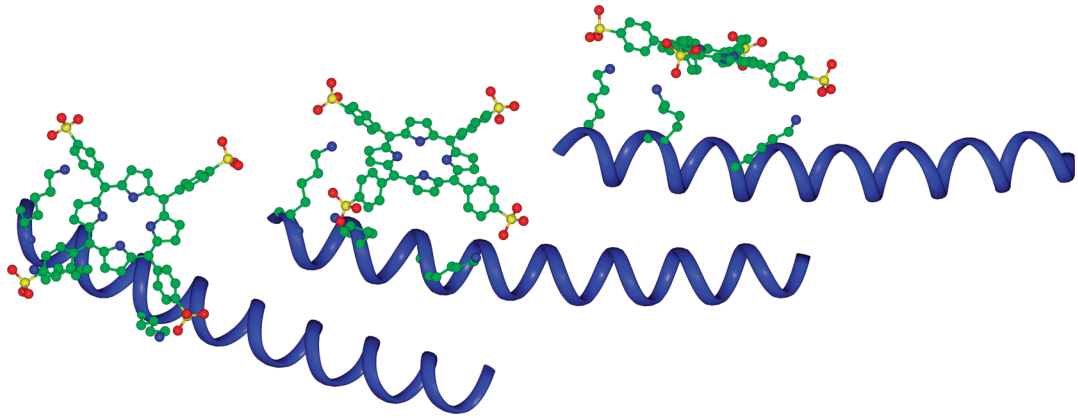

**Figure 1.** Model of Cp3K coiled-coil polymer interacting with $TPPS_4$. The model contains three coiled-coil peptide units (shown in ribbon form) whose backbone representation is taken from the structure that we described for the CpA polymerizing model.[29] The view emphasizes the overlapping nature of the helices with respect to one another. At the sites of overlap, isoleucine and leucine residues at the *a* and *d* heptad positions, respectively (side chains not shown), are projecting toward one another between the helices to provide optimal hydrophobic packing interactions for a dimeric coiled coil. Three lysine residues are shown interacting with three of the four sulfonate groups of each $TPPS_4$ porphyrin and is highlighted in ball-and-stick representation.

were assayed at 30000 rpm at a temperature of 25 °C. Absorbance data were collected using a radial step size of 0.003 cm and delay time of 0 s. Data were analyzed using the DCDT+ program version 2.0.9 28802 (John Philo, Thousand Oaks, Ca). Partial specific volume, density, and viscosity were calculated using SednTerp v. 1.08.[34]

**Atomic Force Microscopy.** AFM data were collected in tapping mode using a Bioscope atomic force microscope (Digital Instruments, Santa Barbara, CA). Samples were prepared in 10 mM Tris-HCl, pH 7.8 at peptide/porphyrin ratios required for complex formation and incubated on freshly cleaved mica (SPI Supplies, West Chester, PA) surface for 10 min at room temperature in a constant humidity chamber. Samples were rinsed briefly in Milli-Q water and allowed to dry under nitrogen.

## Results and Discussion

The Cp3K peptide used in this study contains both a protein polymerization domain and a $TPPS_4$ binding domain as described in the Introduction (sequence is shown in Table 1). We first tested biophysical features of the Cp3K peptide to compare its ability to self-assemble to our earlier published work.[29] As with earlier designs, Cp3K remains largely unfolded at neutral pH in the absence of NaCl as judged by the lack of helix content as measured by circular dichroism experiments (Figure 2A). However, there is a significantly higher helix content as compared to CpA (Table 1), our original design, as judged by an increase in signal intensity at 222 nm and a red-shift of the higher energy band toward 208 nm. One contribution to the enhanced helix content probably arises from weak association of the peptides through the enhanced hydrophobic core, in which we replaced the original cysteines in two *a* heptad positions with isoleucines. This is supported by the finding that CpA-I (Table 1), a related peptide with isoleucine at all *a* positions, also shows increased helix content relative to CpA. We had shown previously that polymerization due to coiled-coil assembly can be induced by the presence of high salt concentrations.[29] Thus, we looked at the sensitivity of self-assembly in the presence of NaCl for Cp3K in comparison to CpA and CpA-I (Figure 2B). As expected, Cp3K becomes more helical as a function of added salt and, as predicted based on the enhanced hydrophobic core, the approach to full helix content occurs at much lower NaCl concentrations (1 M) as compared to CpA (3 M). This increased sensitivity to NaCl is similar to that observed for CpA-I (also around 1 M). Finally, direct

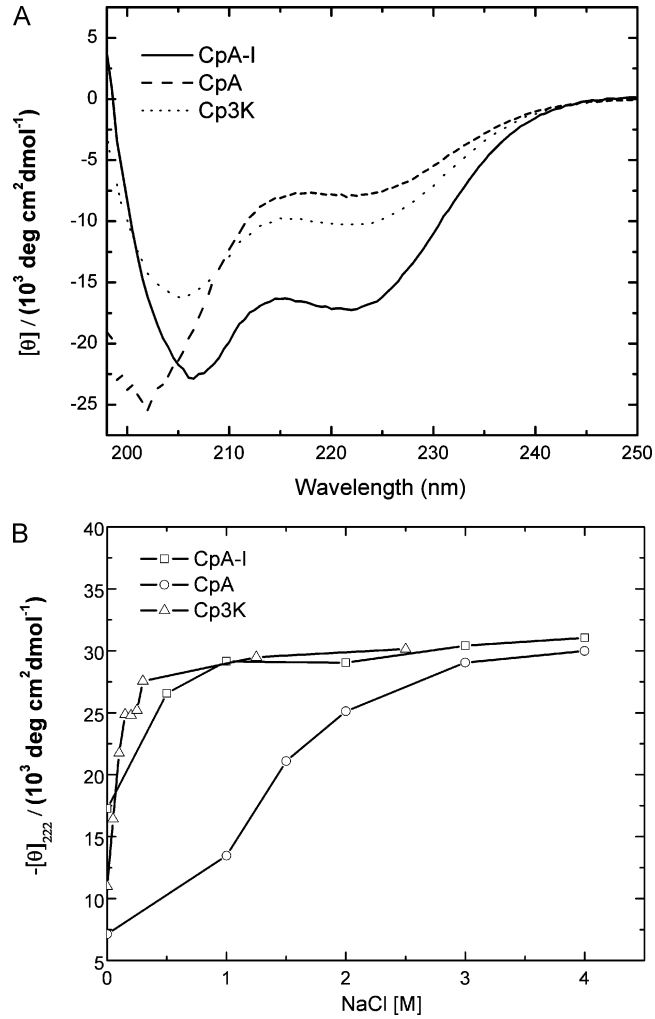


**Figure 2.** Circular dichroism analysis of Cp3K, CpA, and CpA-I. (A) Circular dichroism spectra were taken of 100 $\mu$M each of CpA and Cp3K in 10 mM Tris-HCl, pH 7.8 and measured at 25 °C. (B) NaCl concentration dependence as monitored at 222 nm for each peptide under the same conditions as that reported in (A).

evidence for Cp3K self-assembly in the presence of NaCl was tested by sedimentation velocity analytical ultracentrifugation (SV). Analysis of SV data collected for Cp3K peptide at 100 $\mu$M in 0.1 M NaCl at 25 °C reveals a heterogeneous solution

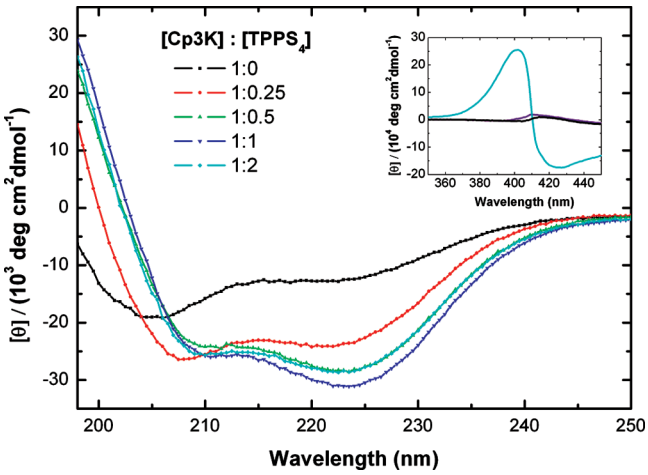


**Figure 3.** Induction of helix content in Cp3K upon addition of $TPPS_4$. Samples were prepared using 20 $\mu$M Cp3K in 10 mM Tris-HCl, pH 7.8 and measured at 25 °C. Inset: CD region of $TPPS_4$ in presence and absence of 50 $\mu$M Cp3K; cyan: 1:2 Cp3K/$TPPS_4$; black: $TPPS_4$ alone, purple: 1:2 Cp3K/$TPPS_4$ with Cp3K in a $\beta$-sheet conformation.

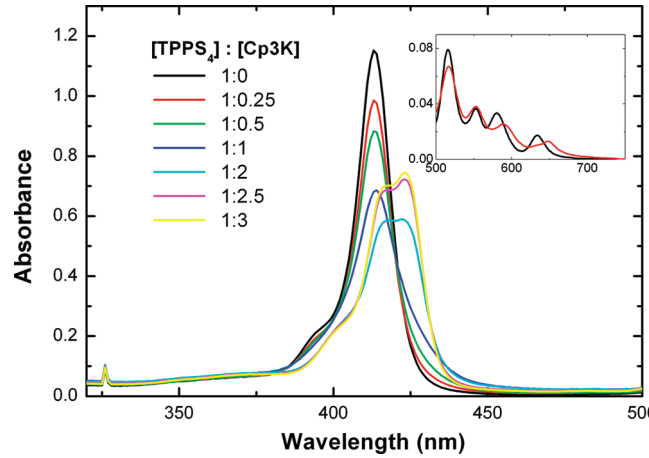


**Figure 4.** Effect of Cp3K binding on $TPPS_4$ absorbance bands. UV−visible absorbance spectra were taken of 20 $\mu$M $TPPS_4$ titrated with increasing Cp3K concentrations (inset: porphyrin $Q_x$-bands). Samples were prepared in 10 mM Tris-HCl, pH 7.8, and measured at 25 °C.

with an average molecular weight distribution in the range of 300 kDa (based on calculations using the best-fit values of $s_{(20,w)}$ of $5.7 \times 10^{-13}$ S, and $D_{(20,w)}$ value of $1.54 \times 10^{-7}$ cm$^2$ s$^{-1}$)), indicating a significant degree of polymerization comparable in size to that observed for our other polymerizing peptides (R.F., unpublished data). AFM images confirmed the presence of polymers for Cp3K in the presence of 0.1 M NaCl but these were quite heterogeneous in their morphology (Figure S1 in Supporting Information), with a broad distribution of heights centered on 2.2 nm.

Interestingly, upon long-term storage of Cp3K stock solutions, there was a conversion to $\beta$-sheet fibrils (based on CD and AFM experiments; see Figures S2 and S3 in Supporting Information). These $\beta$-sheet fibrils are more uniform in their lateral dimensions and quite distinct in their morphology from that observed for the α-helical polymers. We suspect that this propensity to form $\beta$-sheet fibrils is a consequence of the number of glutamines that we engineered into the sequence; such polyglutamine sequences are known to foster $\beta$-sheet fibril self-assembly and their structures have been characterized by AFM.[35,36] This alternative structure was helpful as a control in showing specificity of $TPPS_4$ binding to the α-helical filaments (see below).

Cp3K contains three lysines in the first two hydrophobic heptad repeats, all spaced $i,i+4$ with respect to one another. Based on modeling studies, this spacing facilitates the engagement of three sulfonate groups on an anionic porphyrin, $TPPS_4$, as illustrated in Figure 1. This lysine distribution is identical to that in Cp3K-N, which we had shown previously to become helical upon tight binding of $TPPS_4$.[10] We looked at whether $TPPS_4$ could induce helix content in Cp3K. CD experiments with Cp3K suggest that, upon increasing amounts of $TPPS_4$, the CD spectrum is converted from that representing a largely unfolded structure into an α-helical structure, predicted to contain approximately 91% helix content[37] (Figure 3). There is no contribution to CD in this region of free porphyrin alone. Stoichiometries beyond 1:0.5 Cp3K/$TPPS_4$ result in a red-shifting of both the 208 and 222 bands, suggestive of formation of polymers due to effects on band extinction caused by light scattering.[28] There is also an induced $TPPS_4$ Soret CD band upon peptide binding, suggesting that asymmetry has been imposed on the $TPPS_4$ electronic transitions (Figure 3 inset, cyan line). The intensity of this induced porphyrin band is consistent with that reported elsewhere for a similar structural model system.[38] This CD band is absent in porphyrin by itself (Figure 3 inset, black line). $TPPS_4$ cannot bind to Cp3K when the peptide forms cross-$\beta$-sheet fibrils (Figure 3 inset, purple line), providing additional support that proper juxtaposition of the three lysines in an α-helical conformation is critical for tight binding of $TPPS_4$. The Soret band (normally at 413 nm) is split, resulting in a positive component at 400 nm and a negative component at 424 nm. The absolute magnitudes of these two components are approximately equal in intensity to one another, suggesting that the porphyrins are binding to the peptide in a single conformation. This effect was also observed in binding to our original model system, Cp3K-N, except that the order of the positive and negative bands is reversed upon binding Cp3K-N.[10] We attempted SV experiments on this complex to determine the size of the polymers but the samples precipitated in the time frame of the experiments (6−9 h).

We also studied the effect of the addition of Cp3K on the $TPPS_4$ absorbance bands. At a pH of 7.8, $TPPS_4$ exists in its base form as a monomer with its Soret peak at 413 nm (Figure 4). Upon addition of substoichiometric amounts of Cp3K, we saw a loss in intensity of the 413 nm peak; however, as the peptide concentration exceeds the porphyrin concentration, a new red-shifted peak appears at 425 nm, suggesting evidence for peptide binding[11,13] and possible exciton coupling[39] between bound porphyrins. Red-shifting upon binding was also observed for the porphyrin $Q_x$-bands (Figure 4 inset), providing further support for exciton coupling of porphyrins. In contrast, porphyrin binding to Cp3K-N caused a loss of the 413 nm Soret band with concomitant increase in a blue-shifted peak at 403 nm (Figure 6), as shown in our earlier work.[10] This blue shift is also likely a consequence of changes in the electronic structure of the bound porphyrin, but may also be influenced by H-aggregate type interactions.[14,28,40,41] Unlike the Cp3K-N/$TPPS_4$ two-state binding behavior, as judged by the presence of an isosbestic point in UV−visible titration data,[10] the Cp3K and $TPPS_4$ complex shows multiple-state behavior.

If there is strong exciton coupling of $TPPS_4$ upon addition of Cp3K, we might expect a significant quenching in the fluorescence of the porphyrins bound in the self-assembling polymer. We measured the fluorescence of $TPPS_4$ upon excitation at 413 nm for the porphyrin by itself or in complex with Cp3K (Figure 5). Excitation at 413 nm resulted in fluorescence bands for $TPPS_4$ at

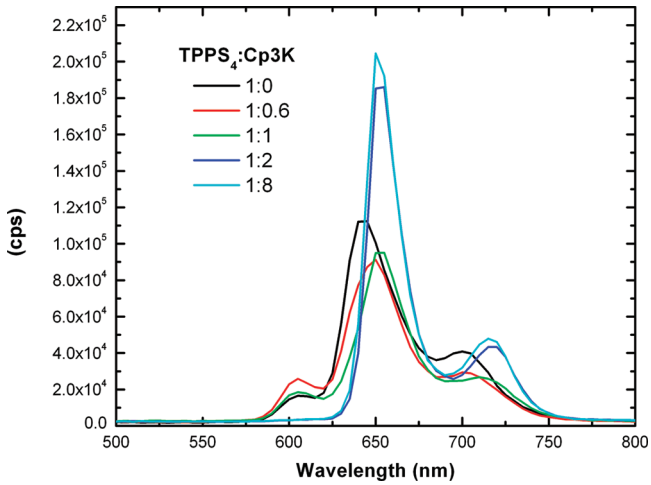


**Figure 5.** Effect of Cp3K binding on TPPS[4] fluorescence. Sample conditions include 5 $\mu$m porphyrin in 10 mM Tris-HCl, pH 7.6.

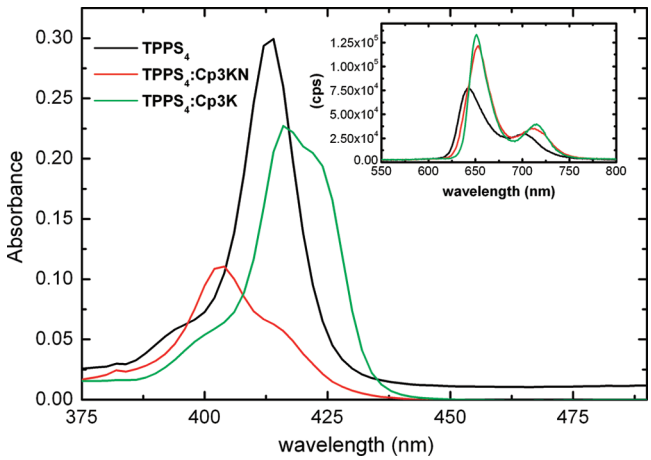


**Figure 6.** Comparison of the absorbance and fluorescence spectra of 5 $\mu$M $TPPS_4$ saturated with 40 $\mu$M Cp3K or Cp3K-N in 10 mM Tris-HCl, pH 7.6.

644 and 705 nm. We observed a slight increase and red-shift in the emission bands upon titration with Cp3K. The red-shifting is most likely due to polymerization effects, as seen in the UV−visible experiment. The separation between the bands also becomes more distinctive. The major band is shifted toward 655 nm and the second band toward 720 nm. The lack of quenching suggests that there is no significant buildup of exciton coupling between porphyrins in the polymeric structure.[11] Interestingly, the emission spectra of $TPPS_4$ in the presence of Cp3K-N and Cp3K are almost identical (Figure 6), providing additional support for minimal exciton coupling.

Because we observed minimal quenching of fluorescence emission, we realized that we could probe directly for $TPPS_4$ binding to the Cp3K filaments by using fluorescence microscopy. Fluorescence microscopy of a 1:1 ratio of $TPPS_4$ to Cp3K showed evidence of large scale aggregation with what look like highly tangled filaments (Figure 7). We suspect that this is what happens when the samples precipitate; we are unlikely to see smaller aggregates due to relatively poor sensitivity of this technique. The smallest polymers that we observed in the field presented in Figure 7 are in the range of 0.1−0.3 $\mu$m, consistent with the size of the polymers observed in AFM images (see below). In the absence of Cp3K, no fluorescence of $TPPS_4$ was observed (data not shown).

To probe the morphology of the Cp3K/$TPPS_4$ polymers at higher resolution, we used AFM imaging. Samples for AFM were

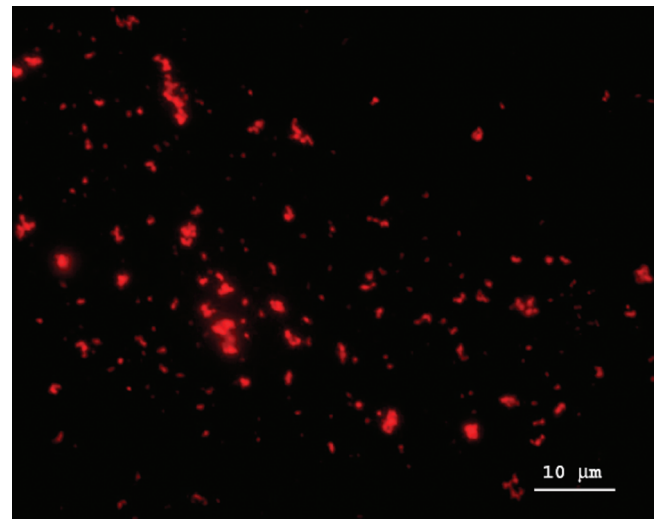


**Figure 7.** Fluorescence microscopy of Cp3K/$TPPS_4$ polymers. Cp3K and $TPPS_4$ at a 1:1 ratio (10 $\mu$M each) in 10 mM Tris-HCl, pH 7.6, were deposited on a freshly cleaved mica surface and incubated in a humidifier box for 10 min at room temperature, rinsed briefly, and then allowed to dry prior to being imaged.

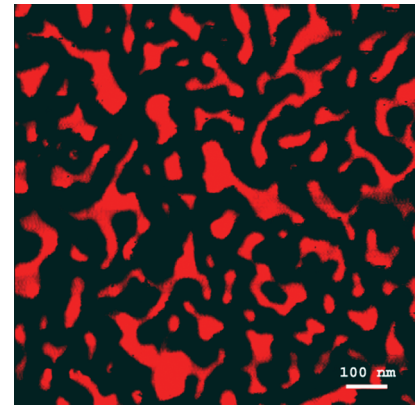


**Figure 8.** AFM topography image of Cp3K/$TPPS_4$ polymers. The AFM image was collected on the sample that was prepared for fluorescence microscopy (see Figure 7).

prepared from the same samples used for the fluorescence microscopy, using a 1:1 ratio of peptide to porphyrin. There is significant heterogeneity in polymer length and some branching is seen, possibly through porphyrin-porphyrin interactions between polymers (Figure 8). Polymer height measurements indicate an average height of 3.52 ± 0.2 nm. Cp3K and CpA polymers in the presence of NaCl have an average height of 2.2 ± 0.6 (determined from an analysis of Figure S1) and 2.9 ± 0.6 nm, respectively.[29] Thus, the difference in height between the polymers in NaCl versus polymers in the presence of $TPPS_4$ is suggestive of porphyrin binding.

## Conclusions

Our goal in this work was to create photoelectronically active biomaterials with atomic level precision of assembly using a coiled-coil polymerizing peptide system and $TPPS_4$, an anionic porphyrin. We show that assembly at the nanoscale mimics the assembly that we observed previously for a soluble peptide/porphyrin system, involving charged interactions between lysine side chains on the peptide and sulfonate groups on the porphyrin.[10] As stated earlier, the advantage of developing this particular binding strategy is to allow us to use different metalated porphyrins without having to

change the design strategy. Because metalation of porphyrins affects their redox properties,[42] it offers a long-term goal for implementing asymmetric addition strategies to create intrinsic voltage potentials across our peptide polymers.

Addition of the porphyrin does not disrupt the designed polymerizing potential of the peptide, as judged by comparing the secondary structure and the polymer morphology to our earlier published work; in fact, it contributes a helix-stabilizing force.[29] Exciton coupling appears to be complex, with UV−visible spectroscopic data supporting such coupling. However, the extent of coupling is weak as evidenced by little fluorescence quenching.

While we have successfully created photoelectronically active biomaterials, the fluorescence microscopy and AFM imaging suggest a significant degree of heterogeneity in polymer length and tangling; this was not entirely unanticipated since we observed a similar degree of heterogeneity in coiled-coil assembly in our earlier work.[29] We argued that the heterogeneity was due in part to the small scale of the filament widths; filaments that aggregate laterally show greater persistence length and overall increased homogeneity in fibril width.[1] Although we intend to pursue rudimentary conductive properties of these materials, we are currently probing environmental conditions to favor the formation of larger, and more regular, fibril structures using our peptide/porphyrin system. Fostering $TPPS_4$ J-aggregate interactions by the addition of coiled-coil forming peptides may result in forming fibril structures with more homogeneous characteristics.[12] Such studies are currently underway.

**Acknowledgment.** We wish to thank Walter Smith and Al Schwab for helpful advice in interpreting the data. We also thank Meg Twomey for able technical assistance and Joe Cammisa for generating the graphics image of the Cp3K/$TPPS_4$ complex. This research was supported by grants from NSF (CHE-0616615 and MCB-0516025 to R.F.), the David and Lucile Packard Foundation to J.C.d.P., K.A.J., and R.F., and grants to Haverford College from the Arnold and Mabel Beckman Foundation and the HHMI Undergraduate Science Education Program to support undergraduate research.

**Supporting Information Available.** Atomic force microscopy image of Cp3K in 0.1 M NaCl and circular dichroism spectrum and atomic force microscopy image of Cp3K peptide forming cross-$\beta$-sheet fibrils. This material is available free of charge via the Internet at http://pubs.acs.org.

## References and Notes

(1) Fairman, R.; Akerfeldt, K. S. *Curr. Opin. Struct. Biol.* **2005**, *15*, 453–463.
(2) Lombardi, A.; Nastri, F.; Pavone, V. *Chem. Rev.* **2001**, *101*, 3165–3189.
(3) Reedy, C. J.; Gibney, B. R. *Chem. Rev.* **2004**, *104*, 617–649.
(4) Pasternack, R. F. *Chirality* **2003**, *15*, 329–332.
(5) Pasternack, R. F.; Gibbs, E. J. *Met. Ions Biol. Syst.* **1996**, *33*, 367–397.
(6) Synytsya, A.; Synytsya, A.; Blafkova, P.; Volka, K.; Kral, V. *Spectrochim. Acta, Part A* **2007**, *66*, 225–235.
(7) Postigo, F.; Mora, M.; De Madariaga, M. A.; Nonell, S.; Sagrista, M. L. *Int. J. Pharm.* **2004**, *278*, 239–254.
(8) Prochazka, M.; Stepanek, J.; Turpin, P. Y. *Chem. Phys. Lipids* **2004**, *132*, 145–156.
(9) Ricchelli, F.; Gobbo, S.; Moreno, G.; Salet, C.; Brancaleon, L.; Mazzini, A. *Eur. J. Biochem.* **1998**, *253*, 760–765.
(10) Kovaric, B. C.; Kokona, B.; Schwab, A. D.; Twomey, M. A.; de Paula, J. C.; Fairman, R. *J. Am. Chem. Soc.* **2006**, *128*, 4166–4167.
(11) Tian, F.; Johnson, E. M.; Zamarripa, M.; Sansone, S.; Brancaleon, L. *Biomacromolecules* **2007**, *8*, 3767–3778.
(12) Valanciunaite, J.; Bagdonas, S.; Streckyte, G.; Rotomskis, R. *Photochem. Photobiol. Sci.* **2006**, *5*, 381–388.
(13) Andrade, S. M.; Costa, S. M. B. *Biophys. J.* **2002**, *82*, 1607–1619.
(14) Ohno, O.; Kaizu, Y.; Kobayashi, H. *J. Chem. Phys.* **1993**, *99*, 4128–4139.
(15) Augulis, R.; Snitka, V.; Rotomskis, R. *Solid State Phenom.* **2004**, *97−98*, 191–194.
(16) Augulis, R.; Valiokas, R.; Liedberg, B.; Rotomskis, R. *Solid State Phenom.* **2004**, *97−98*, 195–200.
(17) Rotomskis, R.; Augulis, R.; Snitka, V.; Valiokas, R.; Liedberg, B. *J. Phys. Chem. B* **2004**, *108*, 2833–2838.
(18) Schwab, A. D.; Smith, D. E.; Rich, C. S.; Young, E. R.; Smith, W. F.; de Paula, J. C. *J. Phys. Chem. B* **2003**, *107*, 11339–11345.
(19) Fleischer, E. B.; Palmer, J. M.; Srivastava, T. S.; Chatterjee, A. *J. Am. Chem. Soc.* **1971**, *93*, 3162–3167.
(20) Pasternack, R. F.; Huber, P. R.; Boyd, P.; Engasser, G.; Francesconi, L.; Gibbs, E.; Fasella, P.; Venturo, G. C.; Hinds, L. D. *J. Am. Chem. Soc.* **1972**, *94*, 4511–4517.
(21) Ribo, J. M.; Crusats, J.; Farrera, J. A.; Valero, M. L. *J. Chem. Soc., Chem. Commun.* **1994**, 681–682.
(22) Aoudia, M.; Guliaev, A. B.; Leontis, N. B.; Rodgers, M. A. J. *Biophys. Chem.* **2000**, *83*, 121–140.
(23) Aoudia, M.; Rodgers, M. A. J. *Langmuir* **2005**, *21*, 10355–10361.
(24) Urbanova, M.; Setnicka, V.; Kral, V.; Volka, K. *Biopolymers* **2001**, *60*, 307–316.
(25) Takahashi, M.; Ueno, A.; Mihara, H. *Chem.—Eur. J.* **2000**, *6*, 3196–3203.
(26) Takahashi, M.; Ueno, A.; Uda, T.; Mihara, H. *Bioorg. Med. Chem. Lett.* **1998**, *8*, 2023–2026.
(27) Venkatesh, B.; Jayakumar, R.; Pandian, R. P.; Manoharan, P. T. *Biochem. Biophys. Res. Commun.* **1996**, *223*, 390–396.
(28) Dunetz, J. R.; Sandstrom, C.; Young, E. R.; Baker, P.; Van Name, S. A.; Cathopolous, T.; Fairman, R.; de Paula, J. C.; Akerfeldt, K. S. *Org. Lett.* **2005**, *7*, 2559–2561.
(29) Wagner, D. E.; Phillips, C. L.; Ali, W. M.; Nybakken, G. E.; Crawford, E. D.; Schwab, A. D.; Smith, W. F.; Fairman, R. *Proc. Natl. Acad. Sci. U.S.A.* **2005**, *102*, 12656–12661.
(30) Woolfson, D. N. *Adv. Protein Chem.* **2005**, *70*, 79–112.
(31) Woolfson, D. N.; Ryadnov, M. G. *Curr. Opin. Chem. Biol.* **2006**, *10*, 559–567.
(32) Gribbon, C.; Channon, K. J.; Zhang, W.; Banwell, E. F.; Bromley, E. H.; Chaudhuri, J. B.; Oreffo, R. O.; Woolfson, D. N. *Biochemistry* **2008**, *47*, 10365–10371.
(33) Rosen, H. *Arch. Biochem. Biophys.* **1957**, *67*, 10–15.
(34) Laue, T. M., Shah, B. D., Ridgeway, T. M., Pelletier, S. L. Computer-Aided Interpretation of Analytical Sedimentation Data for Proteins. In *Analytical Ultracentrifugation in Biochemistry and Polymer Science*; Harding, S. E., Rowe, A. J., Horton, J. C., Eds.; The Royal Society of Chemistry: Cambridge, 1992.
(35) Dahlgren, P. R.; Karymov, M. A.; Bankston, J.; Holden, T.; Thumfort, P.; Ingram, V. M.; Lyubchenko, Y. L. *Dis. Mon.* **2005**, *51*, 374–385.
(36) Poirier, M. A.; Li, H. L.; Macosko, J.; Cai, S. W.; Amzel, M.; Ross, C. A. *J. Biol. Chem.* **2002**, *277*, 41032–41037.
(37) Rohl, C. A.; Baldwin, R. L. *Methods Enzymol.* **1998**, *295*, 1–26.
(38) McAllister, K. A.; Zou, H.; Cochran, F. V.; Bender, G. M.; Senes, A.; Fry, H. C.; Nanda, V.; Keenan, P. A.; Lear, J. D.; Saven, J. G.; Therien, M. J.; Blasie, J. K.; DeGrado, W. F. *J. Am. Chem. Soc.* **2008**, *130*, 11921–11927.
(39) Arai, T.; Inudo, M.; Ishimatsu, T.; Akamatsu, C.; Tokusaki, Y.; Sasaki, T.; Nishino, N. *J. Org. Chem.* **2003**, *68*, 5540–5549.
(40) Parkash, J.; Robblee, J. H.; Agnew, J.; Gibbs, E.; Collings, P.; Pasternack, R. F.; de Paula, J. C. *Biophys. J.* **1998**, *74*, 2089–2099.
(41) Solladie, N.; Aubert, N.; Bouatra, S.; Bourgogne, C.; Bregier, F.; Brettar, J.; Gisselbrecht, J. P.; Gross, M.; Rein, R.; Sooambar, C.; Troiani, V.; Walther, M. *J. Porphyrins Phthalocyanines* **2003**, *7*, 270–281.
(42) Fuhrhop, J.-H. Reversible reactions of porphyrins and metalloporphyrins and electrochemistry. In *Porphyrins and Metalloporphyrins*; Smith, K. M., Ed.; Elsevier Scientific Publishing Company: Amsterdam, 1975; pp 593−666.

BM9000553

# SUPPORTING INFORMATION

# Self Assembly of Coiled-Coil Peptide-Porphyrin Complexes.

*Bashkim Kokona, Andrew M. Kim, R. Claire Roden, Joshua P. Daniels, Brian J. Pepe-Mooney, Brian C. Kovaric, Julio C. de Paula,[§] Karl A. Johnson, and Robert Fairman**

Department of Biology, Haverford College, 370 Lancaster Ave, Haverford, PA 19041

[§]Current Address: Department of Chemistry, Lewis and Clark College, 0615 SW Palatine Hill Rd., Portland, OR 97219

**Figure S1.** Tapping-mode AFM images of 100 µM Cp3K in 10 mM Tris-HCl, pH 7.8 and 0.1 M NaCl.

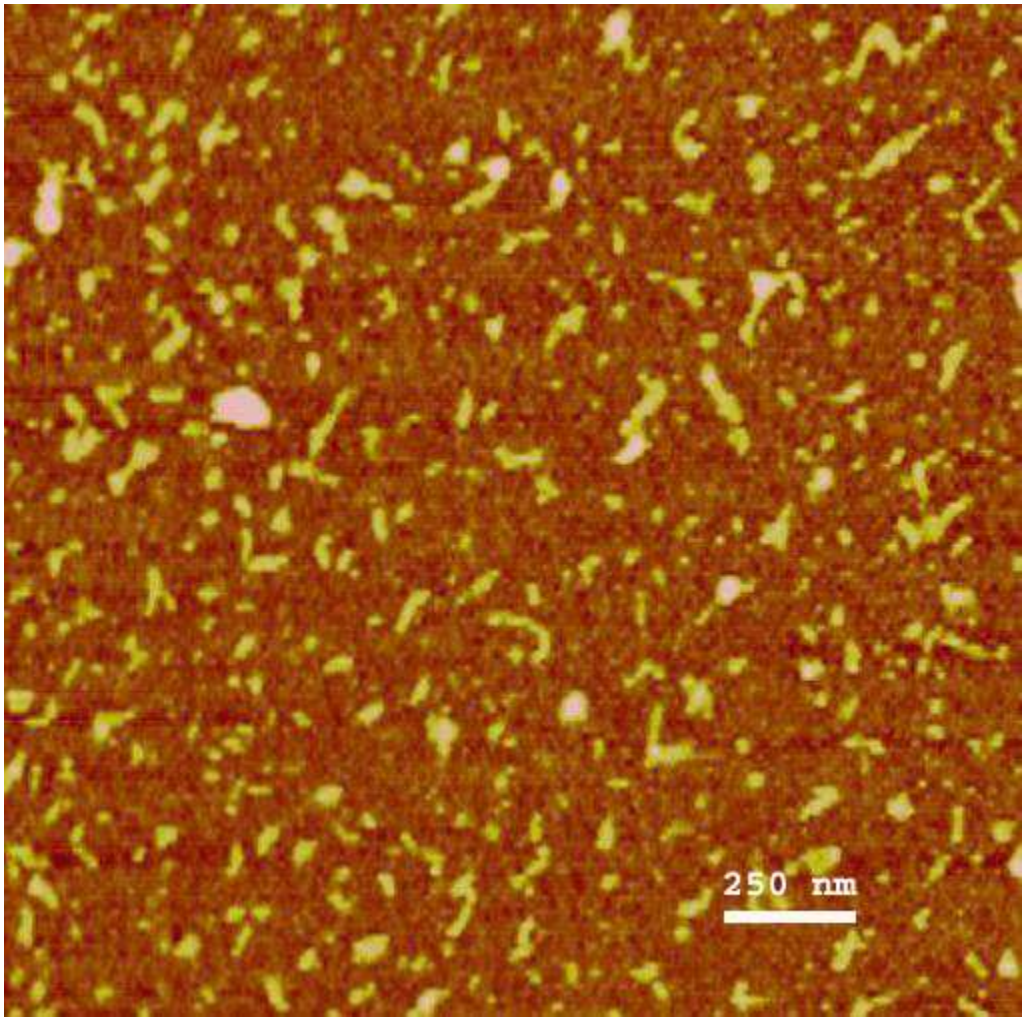

**Figure S2.** CD spectra of Cp3K in α-helix and β-sheet conformations. Cp3K concentration is 100 μM in 10mM Tris-HCl, pH 7.8 prepared with fresh stock solution and aged stock solution.

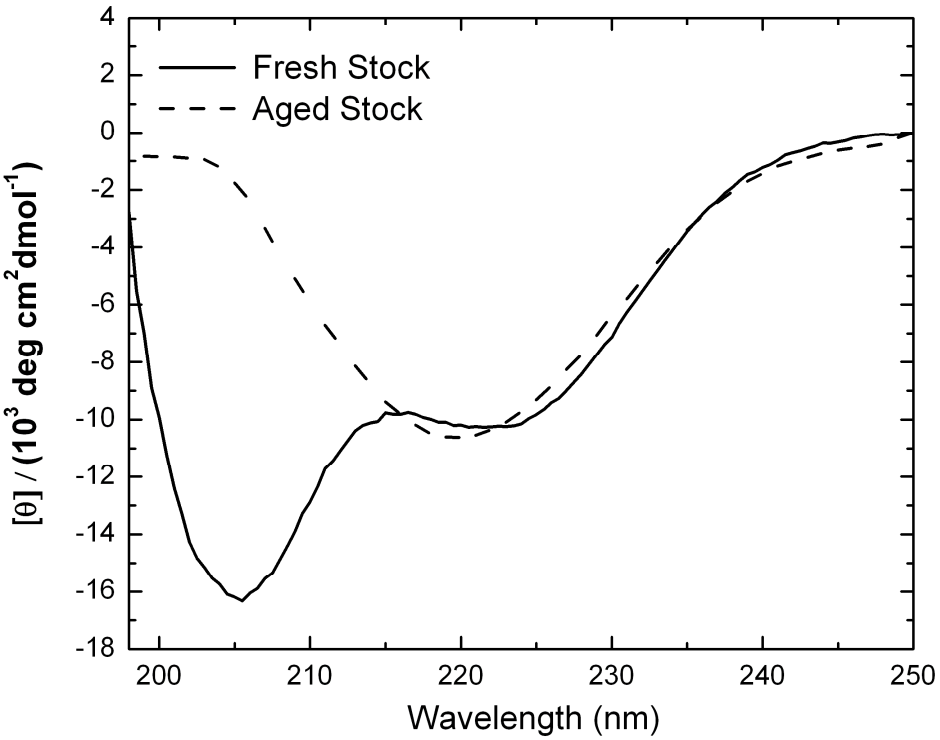

**Figure S3.** Tapping-mode AFM image of 100 μM Cp3K in cross-β-sheet fibril conformation.